Characteristic Dependency of Hydrogen-Affected Fatigue Crack Growth and Crack Tip Plasticity on Low Loading Frequency in α-Iron

TOMOKI SHINKO, GILBERT HÉNAFF, DAMIEN HALM, GUILLAUME BENOIT, and HADI BAHSOUN

Aiming to investigate the dependency of hydrogen-affected fatigue crack growth (HAFCG) on the loading frequency f, this study experimentally characterized the HAFCG in a commercially pure iron as a function of f ranging from 0.02 to 20 Hz as well as a stress intensity factor range ΔK and hydrogen gas pressure P_{H_2}. The crack tip plasticity was analyzed by interferometric microscopy and transmission electron microscopy in addition to the fracture surface observation. As a result, the amount of FCG rate acceleration by hydrogen increases as f decreases until it reaches a critical value ($f = 2$ Hz at $P_{H_2} = 3.5$ MPa, $f = 0.2$ Hz at $P_{H_2} = 35$ MPa), while the HAFCG rate greatly decreases once f decreases below the critical value. At the same time, the fracture mode at $P_{H_2} = 3.5$ MPa changes from brittle quasi-cleavage to a more ductile manner showing no clear hydrogen influence. On the other hand, the size of cleavage-like facets becomes large in case of $P_{H_2} = 35$ MPa suggesting that the number of lattice planes causing cleavage is reduced because of less hydrogen effect. The crack tip plasticity reduction by hydrogen is clearly confirmed while the HAFCG enhancement occurs above the critical value of f. In contrast, at f below the critical value, the crack tip plasticity is recovered to almost the same level as in the inert environment. Based on a theoretical estimation of hydrogen diffusion from the crack tip, the critical value of f causing this reversal f dependency is likely determined by the hydrogen concentration gradient in the vicinity of the crack tip. Although the associated mechanism is still unclear, it is suggested that the dynamic interaction between mobile dislocations and diffusing hydrogen atoms is important in clarifying the mechanism of HAFCG.

I. INTRODUCTION

IN recent years, the use of hydrogen energy has been spreading, aiming toward the realization of a sustainable society without dependence on fossil fuels. Along with this, the number of kinds of equipment handling high-pressure gaseous hydrogen is increasing. However, a crucial problem when using hydrogen-related equipment is hydrogen embrittlement (HE),[1–4] which induces a degradation of metallic material strength. In particular, the decrease in fatigue strength of metallic materials in a hydrogen gas environment is significant.[2,5] This is a major problem in long-term use of hydrogen-related equipment.

Since the discovery of HE by Johnson[6] in 1874, much research on this topic has been conducted. Among the many proposed HE mechanisms, the following four are widely recognized: Hydrogen-Enhanced DEcohesion (HEDE),[7,8] Hydrogen-Enhanced Localized Plasticity (HELP),[9] Adsorption-Induced Dislocation Emission (AIDE),[10] and Hydrogen-Enhanced Strain-Induced Void (HESIV).[11] HEDE is a mechanism that promotes brittle fracture because of interatomic bonding weakened by interstitial hydrogen in front of the crack tip. HELP is a mechanism assuming that plastic deformation in the vicinity of the crack tip is enhanced and localized by solute hydrogen atoms. The AIDE mechanism is based on a promotion effect for dislocation nucleation and emission by adsorbed hydrogen atoms on the crack surface. The HESIV mechanism suggests that microscopic ductile fracture occurs by solute hydrogen in front of the crack tip promoting microvoid nucleation and coalescence. Recent understandings of the condition in which each mechanism is activated and how they influence crack growth as a result of their combination are well summarized in a review paper by

TOMOKI SHINKO, GILBERT HÉNAFF, DAMIEN HALM, GUILLAUME BENOIT, and HADI BAHSOUN are with the Department of Physics and Mechanics of Materials, Prime Institute, UPR 3346 CNRS - ISAE-ENSMA - Université de Poitiers, Téléport 2 – 1 avenue Clément Ader, Futuroscope Chasseneuil Cedex, 86961, France. Contact e-mail: shinko3755@criepi.denken.or.jp
Manuscript submitted January 13, 2020.
Article published online June 11, 2020.

Djukic et al.[4] Several interpretations such as independent action or coexistence of the above four mechanisms have been given through numerical simulations [12–15] and experimental studies on different steels such as low-carbon steel,[16,17] dual-phase steel,[18] ultra-high strength steel,[19,20] martensitic steel,[21,22] martensitic stainless steel,[23] and iron.[24–27]

The above models attempt to explain the effects of hydrogen dissolved in the crack tip region on crack growth under a monotonic loading condition. On the other hand, in recent years, vigorous research has been conducted to elucidate an HE effect on fatigue crack under cyclic loading. The complexity and difficulty of the hydrogen-affected fatigue crack growth (HAFCG) problem is because of the presence of many influential factors such as crack tip stress intensity factor range ΔK, hydrogen gas pressure P_{H_2} (or hydrogen concentration), and loading frequency f. The authors' previous study systematically demonstrated that these three factors induce complex changes in the Hydrogen-Affected Fatigue Crack Growth Rate (HAFCGR) and fracture morphology.[27] It has been elucidated that characteristic hydrogen-induced intergranular fracture occurs at low ΔK in pure iron under hydrogen gas environment. Its mechanism can be interpreted as the voids coalesce along the grain boundary induced by the accumulation of hydrogen atoms intensively transported by the mobile dislocations, evidenced by experimental [24,27] and numerical studies.[25,26] Meanwhile, if ΔK exceeds a certain value, the fracture mode changes into a brittle transgranular fracture, and the fatigue crack growth rate (FCGR) greatly increases. The higher P_{H_2} is, the lower the threshold value of ΔK at which the fatigue crack growth (FCG) acceleration begins. The lower the loading frequency is, the greater the acceleration amount of the FCGR in the high ΔK region. Four models have been proposed to explain the hydrogen-induced brittle transgranular fracture under a high-stress intensity amplitude: (1) the Hydrogen-Enhanced Successive Fatigue Crack Growth (HESFCG) model,[28,29] (2) hydrogen-induced void-coalescence model,[30] (3) hydrogen-induced cyclic cleavage model,[27,31,32] and (4) HELP + HEDE synergistic model.[4,16,33]

First, the HESFCG model was proposed by Matsuoka et al.[28,29] who optically observed the vicinity of fatigue cracks in a hydrogen environment and found that the size of the plastically deformed zone around the crack tip is greatly reduced by the presence of hydrogen. This model assumes that the part where slip occurs at the crack tip is localized by hydrogen with the HELP mechanism, and the crack tip is sharpened. Along with this, the opening angle of the stretch zone decreases, and the crack growth rate increases up to the stretch zone width.

Second, the hydrogen-induced void-coalescence model was proposed by Nishikawa et al.[30] This model assumes that the interaction between hydrogen and the plastically deformed zone ahead of the crack tip produces dense microvoids by the HESIV mechanism. Consequently, ductile tearing occurs between microvoids, leading to microvoid coalescence and crack growth.

Third, the hydrogen-induced cyclic cleavage model was originally proposed by Marrow et al.[34] and has been further developed by the authors [35] and Birenis et al.[31,32] The authors [35] performed a surface topography measurement near the hydrogen-affected fatigue crack path in pure iron by interferometric microscopy as well as a dislocation structure observation immediately beneath the fracture surface by a transmission electron microscopy (TEM). It has been found that the crack tip plasticity is clearly reduced by hydrogen within a range of a few hundred micrometers from the crack tip. Crack tip plasticity reduction was also observed immediately beneath the fracture surface as the dislocation structure was less developed in hydrogen than in an inert environment. Birenis et al.[31,32,36] drew similar conclusions from their experimental studies with pure iron. In addition, they identified that the hydrogen-induced transgranular crack path tends to follow the weakest lattice plane (i.e., cleavage plane). Based on these experimental facts, the model has been proposed to describe the HAFCG mechanism as follows. When the hydrogen concentration in front of the crack tip and the crack tip stress intensity reach a certain level, cleavage fracture occurs across the crystal because of a weakening effect of atomic bonds by the HEDE mechanism. The achievement of this high hydrogen concentration and stress state may be a consequence of different hydrogen effect such as a dislocation mobility suppression effect by solute hydrogen.[37–42]

Finally, Djukic et al.[4,16] proposed the concept of a coexistence and synergistic actions of HELP and HEDE (the HELP + HEDE synergistic model) based on many references as well as their own experimental investigation. This concept suggests that the dominant HE mechanism changes from HELP to HEDE under increasing hydrogen concentration and/or applied stress state. In the HELP dominant state, hydrogen-enhanced plasticity mediates an achievement of high hydrogen concentration at the crack tip to activate the decohesion fracture process (namely, HELP-mediated HEDE model). Reaching a critical hydrogen concentration, the fracture mode drastically changes to decohesion-controlled fracture manner (i.e., HEDE dominance) because of hydrogen impeding plasticity. This model is in good agreement with the significance of the HELP mechanism even for the decohesion process highlighted by Martin et al.[33] The synergy and competition of those two HE mechanisms have also been suggested by Ogawa et al.[24,43]

The above models (1) through (3) basically correlate the hydrogen effect with only one HE mechanism, while model (4) assumes a combination of two different HE mechanisms (HELP and HEDE). Although these models have been proposed so far, a common agreement on the mechanism has not been obtained yet since many questions remain on the mechanism of HAFCG, which involves complex multi-factor dependencies as described above.

Yoshikawa et al.[44,45] reported an interesting finding regarding the dependency of HAFCG on loading frequency. In the FCG test on carbon steel under a hydrogen gas environment, the FCGR increases with a

decrease in the loading frequency down to a certain value, while if the loading frequency becomes lower than a certain value, the FCGR sharply decreases and the acceleration effect by hydrogen almost disappears. This result is surprising because it was not expected from the conventional understanding that a lower loading frequency always induces a higher FCGR enhancement or saturation.[46–50] Yoshikawa et al. also suggested that this f dependency may be controlled by the gradient of the hydrogen concentration ahead of the crack tip. However, its mechanism has not been clarified because of a shortage of investigations of this phenomenon. No detailed analysis of the crack tip plasticity of HAFCG at such low f has been made, which is indispensable to understand the f dependency of HAFCG.

A purpose of this study is to further investigate the dependence of HAFCG on f as well as P_{H_2} and to understand its mechanism. To this end, FCG tests with ΔK-increasing and ΔK-constant conditions under gaseous hydrogen environment were performed in a commercially pure iron at loading frequencies down to 0.02 Hz, which is lower than the ones applied in a previous study.[27] The fracture surface, plastic strain distribution around the crack tip and dislocation structure immediately beneath the fracture surface were analyzed by means of scanning electron microscopy (SEM), an interferometric microscopy, and TEM, respectively. Based on the obtained results, the mechanism of acceleration of the crack growth rate by hydrogen, the f dependency of HAFCG, and its criteria are discussed.

II. MATERIAL AND TESTING METHOD

A commercially pure iron, Armco iron (AK Steel Corp.) was used in this study. Table I shows the chemical composition of Armco iron. The material was annealed at 1073 K (800 °C) for 60 minutes to remove residual stress and homogenize the ferrite microstructure. The average grain size is approximately 90 μm. Yield strength, maximum elongation, and tensile strength are σ_y = 170 MPa, A = 25 pct, and σ_{TS} = 280 MPa, respectively.

Specimen geometry and the test procedure followed ASTM standard E647. Compact tension (C(T)) specimens with a width W = 40 mm and thickness B = 8 mm were machined in the longitudinal–transversal (L–T) plane against the hot-rolling direction. The specimen surface was finished by buffing with diamond abrasives of 1 μm diameter.

Table I. Chemical Composition of Armco Iron (Mass Percent)

Element	C	Mn	P	S	Cu	N	Al
Content	0.001	0.050	0.003	0.003	0.009	0.004	0.005
Element	Cr	Mo	Ni	Sn	Si		Fe
Content	0.015	0.002	0.14	0.002	0.004		balance

The FCG tests were performed by a loading control under ΔK-increasing and ΔK-constant conditions. The ΔK-increasing FCG test is an FCG test that keeps the load amplitude constant; thus, the ΔK value gradually increases with increasing crack length. On the other hand, the ΔK-constant FCG test was conducted by controlling (gradually decreasing) the applied loading to maintain ΔK at a constant value. The tests were periodically stopped, and the crack length was measured optically. Next, the loading amplitude was changed to maintain ΔK within the range of 20 ± 0.5 MPa × $m^{1/2}$. This method is useful for obtaining the FCGR at low loading frequency with reasonable testing time, since this method requires a short crack extension (such as 1 mm) at one loading frequency. The stress ratio (K_{min}/K_{max}) was 0.1, where K_{min} and K_{max} are the minimum and maximum stress intensity factors, respectively.

All the tests were performed on a Hycomat test bench [46] developed by Pprime Institute. This test bench consists of a high-pressure gas chamber and a hydraulic fatigue testing machine. Hycomat can perform mechanical tests at a maximum gas pressure of 40 MPa at a maximum temperature of 150 °C (423 K). For the ΔK-increasing FCG test, the test environment was gaseous hydrogen at a pressure of P_{H_2} = 3.5. The loading frequency f was 0.2 Hz. The direct current potential drop (DCPD) technique was applied to measure the crack length. For the ΔK constant FCG tests, gaseous nitrogen at pressure P_{N_2} = 3.5 MPa and gaseous hydrogen at pressures P_{H_2} = 3.5 and 35 MPa were applied. The loading frequencies f were 0.02, 0.2, 2, and 20 Hz. The crack length was measured optically using a long-range microscope. The amounts of water vapor and oxygen contained in hydrogen gas at 1 bar were 18 and 10 ppm, respectively.

III. RESULT

A. Fatigue Crack Propagation Rate

Figure 1 presents the FCGR-ΔK relationship for ΔK-increasing FCG tests at hydrogen gas pressure P_{H_2} = 3.5 MPa and loading frequency f = 0.2 Hz (indicated by *), in addition to the previously obtained results at P_{H_2} = 3.5, 35 MPa and f = 0.2, 2, 20 Hz as well as inert environments (air, nitrogen and vacuum).[27,47,48] The FCGR curve in hydrogen can be divided into three regimes according to its shape as indicated by the regimes (a) through (c) for the curve at f = 0.2 Hz and P_{H_2} = 35 MPa, for example, in the figure. Regimes (a) through (c) are called the non-accelerated regime, transition regime and accelerated regime, respectively. The HAFCGR is the same level as in air in the non-accelerated regime, while the HAFCGR rapidly increases in the transition regime until its gradient comes back to the same level as in air in the accelerated regime. The fracture type and crack tip plasticity in these three regimes were investigated in the previous study.[27]

Comparing the FCGR curves at f = 2 Hz, P_{H_2} = 3.5, and 35 MPa to see the hydrogen gas pressure effect, the ΔK value at the beginning of the transition regime, noted

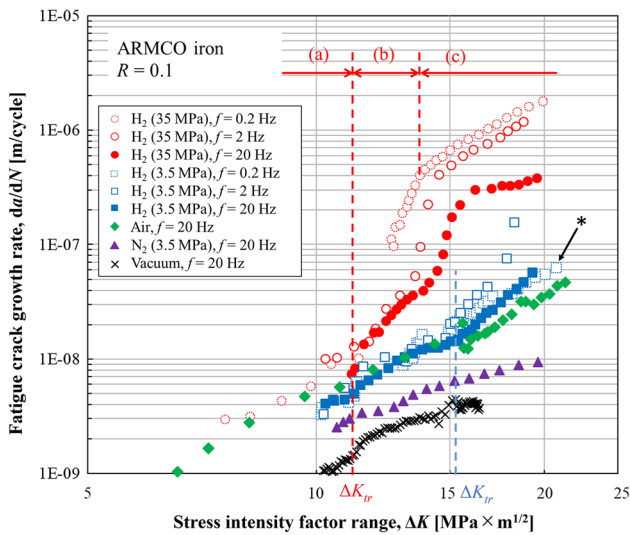Fig. 1—FCGR vs ΔK curves of the tests at f = 0.2, 2, and 20 Hz under gaseous hydrogen at P_{H_2} = 3.5 and 35 MPa as well as the ones in inert environments.[27,47,48] Regimes (a) to (c) represent the non-accelerated regime, transition regime, and accelerated regime, respectively.

ΔK_{tr}, at P_{H_2} = 35 MPa is lower (ΔK_{tr} ~ 11 MPa × $m^{1/2}$) than that at P_{H_2} = 3.5 MPa (ΔK_{tr} ~ 15 MPa × $m^{1/2}$).

In terms of the influence of loading frequency, at P_{H_2} = 35 MPa, higher FCGR enhancement occurs at lower frequency. On the other hand, at P_{H_2} = 3.5 MPa, the FCGR at f = 2 Hz is higher than that at f = 20 Hz, but the FCGR at f = 0.2 Hz is much lower than that at f = 2 Hz. Interestingly, the effect of loading frequency on FCGR at P_{H_2} = 3.5 MPa is reversed below f = 2 Hz, and the transition regime does not clearly appear. This result is consistent with the finding of Yoshikawa et al.[44,45] mentioned in the Introduction. They observed this type of hydrogen effect attenuation at constant ΔK of 30 MPa × $m^{1/2}$. The present result over a wide range of ΔK additionally suggests that the hydrogen effect attenuation is a result of disappearances of the transition regime and the accelerated regime. To clarify the mechanism of this FCG enhancement attenuation at low loading frequency, further investigation of FCGR in hydrogen at loading frequency < 0.2 Hz is necessary. For this reason, the ΔK-constant FCG tests were performed over a wider range of loading frequency including 0.02 Hz.

Figure 2 presents the FCGRs of ΔK-constant FCG tests at ΔK = 20 MPa × $m^{1/2}$ under hydrogen, air, and nitrogen as a relationship between the FCGR and the loading frequency as well as the results of ΔK-increasing FCG tests. The fracture type and dislocation structure type corresponding to each test result are also indicated, which are explained in Sections III–B and III–C, respectively. The FCGRs in air and nitrogen are lower than those in hydrogen at any loading frequency. Also, the FCGRs in nitrogen increase slightly when the loading frequency is decreased from 20 to 0.02 Hz, but this increment is very small in terms of the order of magnitude.

On the other hand, in hydrogen at P_{H_2} = 35 MPa, the FCGRs increased by decreasing the loading frequency from 20 to 0.2 Hz. In contrast, the FCGR decreased by decreasing the loading frequency from 0.2 to 0.02 Hz. In case of P_{H_2} = 3.5 MPa, though the ΔK-increasing and the ΔK-constant FCG tests exhibit different FCGRs, the FCGRs in both tests increased as the loading frequency decreased down to 2 Hz. Once the loading frequency decreases to 0.2 or 0.02 Hz, the FCGRs drastically decreased by an order of magnitude and became almost the same level as in nitrogen. The attenuation of FCGR enhancement has also been confirmed at P_{H_2} = 35 MPa with a low loading frequency of 0.02 Hz, as well as the case with P_{H_2} = 3.5 MPa.

Some FCGRs of ΔK-constant tests are higher than those of the ΔK-increasing tests with the same testing condition. This difference may be due to the difference in testing method. Indeed, the ΔK-increasing test was performed without interrupting the test. On the other hand, in the ΔK-constant tests, the FCG test was periodically interrupted during the test to change the loading parameters. The average duration of the interruption was 9.5 and 5.7 hours for the tests at P_{H_2} = 3.5 and 35 MPa, respectively. During the interruption time, hydrogen may diffuse into the specimen. For this reason, in the ΔK-constant test, the amount of hydrogen concentration in the vicinity of the crack tip becomes higher than in the ΔK-increasing test. A higher amount of hydrogen concentration probably results in a higher FCGR.

The f dependence is also characterized by an upper limit of the FCGR enhancement. This upper limit of the FCGR has been highlighted by several studies.[28,45,51–53] An upper limit and a corresponding loading frequency depend on the hydrogen gas pressure [45] or pre-charged hydrogen content.[53] Furthermore, a research group at Kyushu University [44,45,53–55] reported that similar HAFCGR reduction occurs at relatively low hydrogen gas pressure (P_{H_2} < 10 MPa) in several types of steel. They also found that the loading frequency causing this reduction of FCGR depends on the hydrogen gas pressure.

B. Fracture Surface Observation

The fracture surface of the specimen was observed by SEM aimed at identifying the fracture mode. Although not shown here, the fracture mode in nitrogen at both f = 20 Hz [27] and 0.02 Hz was confirmed as a ductile-type fracture surface. Figure 3 shows the fracture surfaces of the ΔK-constant tests conducted at ΔK = 20 MPa × $m^{1/2}$ in hydrogen at P_{H_2} = 35 MPa and f = 0.02 (a), 0.2 (b), 2 (c), and 20 Hz (d). This observation revealed that the fracture modes at all the loading frequencies were brittle quasi-cleavage (QC) fracture with some cleavage-like facets and many tear ridges as presented in Figure 3. If one compares the fracture surfaces between f = 0.02 Hz (Figure 3(a)) and higher loading frequencies (Figures 3(b) through (d)), the size of flat surface parts (i.e., cleavage-like facets) at f = 0.02 Hz is relatively larger and flatter (for example, see the marked part in
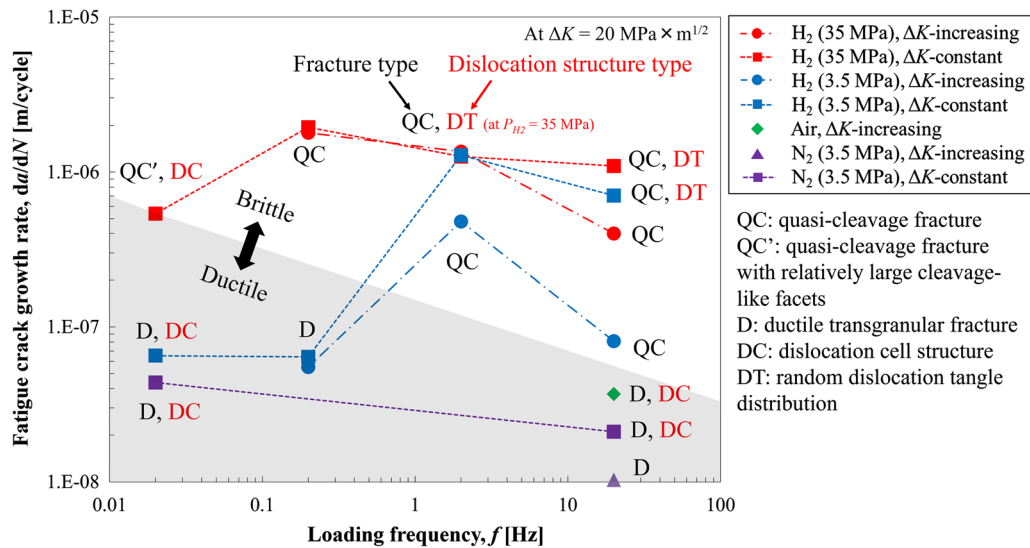
Fig. 2—FCGR *vs* ΔK curves of the ΔK-constant and ΔK-increasing tests at f = 0.02, 0.2, 2, and 20 Hz under gaseous hydrogen at P_{H_2} = 3.5 and 35 MPa as well as the tests in inert environments. This figure also presents the types of fracture mode and dislocation structure for each result of the FCG test.

Figure 3(a)). The fracture surfaces at f = 0.2 to 20 Hz (Figures 3(b) through (d)) are almost covered by a step-like surface morphology consisting of multiple cleavage planes. The distinction between QC and QC' fracture types will be discussed in Section IV–B. The difference in surface appearance between f = 0.02 Hz and higher f is likely related to the difference in FCGR (Figure 2), though both fracture modes are basically the same as brittle QC fracture.

Figure 4 shows fracture surfaces of the ΔK-constant tests at ΔK = 20 MPa × m$^{1/2}$ at P_{H_2} = 3.5 MPa and f = 0.02 (a), 0.2 (b), 2 (c), and 20 Hz (d). The fracture surfaces at f = 0.02 and 0.2 Hz exhibit a relatively ductile fracture (Figures 4(a) and (b)), while the fracture surfaces at f = 2 and 20 Hz represent a brittle QC fracture surface (Figures 4(c) and (d)).

A correlation between the fracture modes and the FCGRs at various f is presented in Figure 2. QC, QC', and D in this figure stand for each fracture mode: quasi-cleavage fracture and quasi-cleavage fracture with relatively large cleavage-like facets and ductile trans-granular fracture, respectively. Interestingly, the ductile fracture corresponds to a relatively low FCGR, while the brittle (QC) fracture corresponds to a relatively high FCGR as indicated in Figure 2. Thus, the QC fracture is clearly associated with the FCGR enhancement effect of hydrogen, while FCG behavior with low FCGR became similar to that of ductile fracture in nitrogen. To elucidate the mechanism of this peculiar f dependency, crack tip plasticity was investigated in the next section.

C. *Crack Tip Plasticity Analysis*

Lateral surface topography near the crack path was measured by an interferometric confocal microscopy (Talysurf CCI6000, Taylor Hobson) to visualize the plastically deformed zone around the crack tip. The surface topographic images of the side surface near the

crack path for the ΔK-constant tests in nitrogen (P_{N_2} = 35 MPa) at f = 0.02 (a) and 20 (b) Hz are presented in Figure 5. This figure indicates the heterogeneous surface unevenness (*i.e.*, out-of-plane displacement, OPD) around the crack path at both loading frequencies. The degree of cyclic plastic deformation at 0.02 Hz appears to be slightly higher than that at 20 Hz.

However, Figure 6 shows the results at P_{H_2} = 3.5 Mpa. In this figure, each image from (a) to (d) corresponds to a different loading frequency f = 0.02, 0.2, 2, and 20 Hz, respectively. The surface unevenness is small at f = 20 Hz, while it slightly develops at f = 2 Hz and is significantly developed at f = 0.02 and 0.2 Hz. Although not shown here, the surface unevenness at P_{H_2} = 35 Mpa is very small at the loading frequencies from 0.2 to 20 Hz; meanwhile, a larger extent of surface unevenness exists at f = 0.02 Hz.[27]

These results from OPD measurement confirm that hydrogen significantly reduces cyclic crack tip plasticity in the accelerated regime associated with FCGR enhancement, while crack tip plasticity becomes noticeable at very low loading frequency (at P_{H_2} = 35 Mpa, f = 0.02 Hz and at P_{H_2} = 35 Mpa, f = 0.2) with the FCGR enhancement attenuation. Therefore, the reduction in cyclic crack tip plasticity is clearly associated with the mechanism of hydrogen-induced FCGR enhancement.

After characterizing the cyclic crack tip plasticity by the above surface topography measurements, TEM observation was applied to investigate the dislocation substructure as a microscopic plasticity indicator under the influence of hydrogen gas pressure and the loading frequency. Figure 7 presents the observations of the ΔK-constant tests at ΔK = 20 Mpa × $m^{1/2}$ in hydrogen of P_{H_2} = 35 Mpa at f = 20 (a) and (b) and 0.02 Hz (c) and (d). The foil extraction location corresponding to f = 20 Hz (Figure 7(a)) is on a cleavage-like facet covered with brittle striations. The dislocation structure
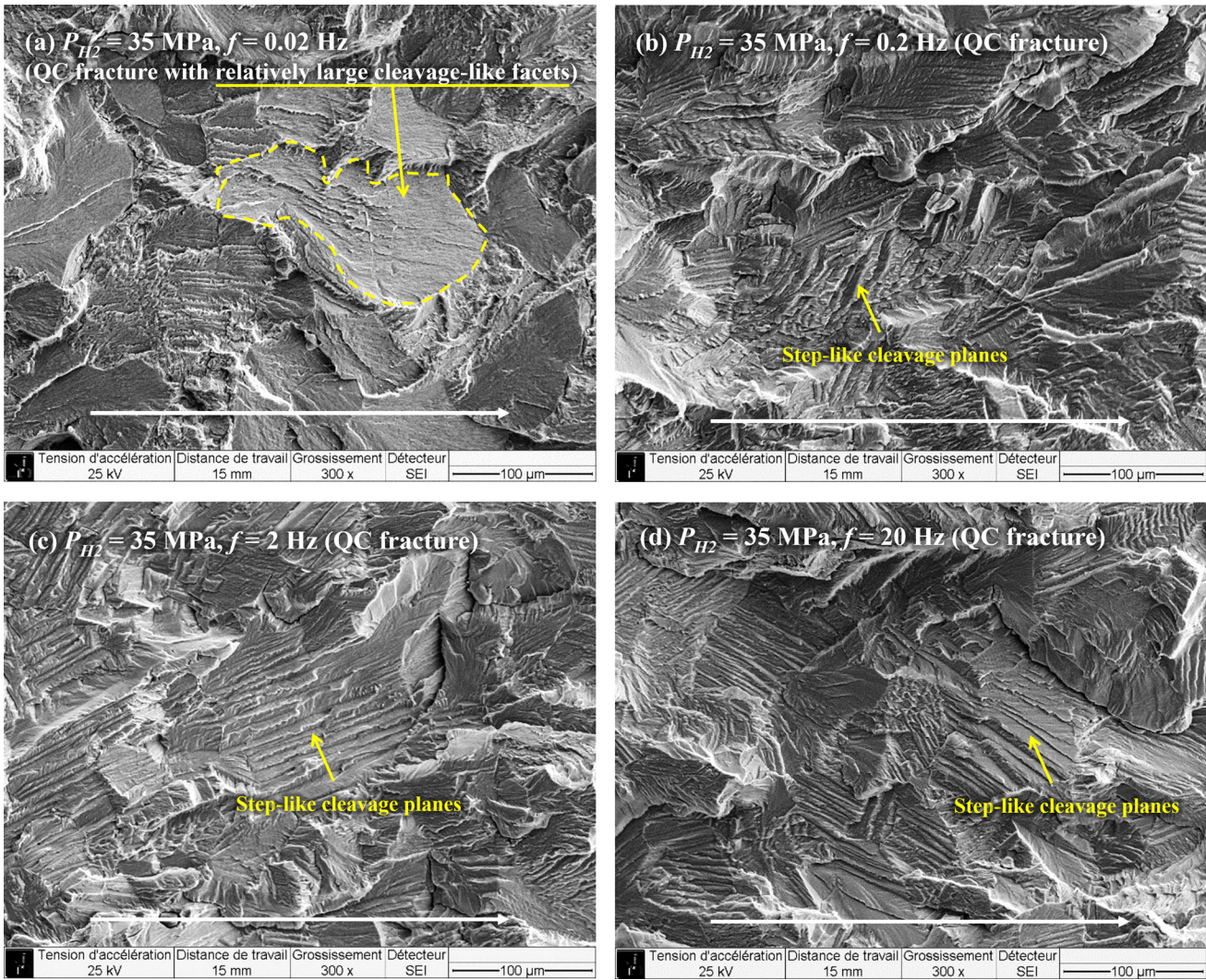
Fig. 3—Fracture surfaces of the ΔK-constant tests (at $\Delta K = 20$ MPa $\times m^{1/2}$) in hydrogen at $P_{H_2} = 35$ MPa and $f = 0.02$ (*a*), 0.2 (*b*), 2 (*c*), and 20 Hz (*d*). The crack propagation direction is from left to right.

immediately beneath the fracture surface (Figure 7(b)) appears to be composed of a random distribution of low density dislocation tangles. Two dislocation walls indicated by red arrows in the figure can also be noticed. The same type of dislocation structure was confirmed by previous observations for ΔK-increasing tests.[35] On the other hand, at 0.02 Hz, the fracture surface at the extraction location (Figure 7(c)) is a ductile transgranular fracture surface. The global dislocation structure (Figure 7(d)) is a cell structure, but some cell walls are not connected to each other. The difference in the dislocation structures shows the different level of local microscopic plastic strain introduced at the crack tip. The random distribution of dislocation tangles observed at $f = 20$ Hz (Figure 7(b)) is a result of low plastic strain insufficient to form the dislocation cell structure; meanwhile, that achieved at $f = 0.02$ Hz (Figure 7(d)) as the cell structure is well formed. A similar dislocation structure as a result of the presence of hydrogen is confirmed in several references in iron,[31,36,56] low carbon steel,[57,58] and Fe-Al alloy.[59]

Figure 8 presents the dislocation structure of specimens tested at a lower hydrogen gas pressure ($P_{H_2} = 3.5$ Mpa), $f = 20$ (a) and (b), and 0.02 Hz (c) and (d). The extraction position at $f = 20$ Hz (Figure 8(a)) was chosen for a cleavage-like facet with striations. The observed dislocation structure (Figure 8(b)) is a distribution of dislocation tangles that do not have well-defined structure such as a cell. Besides, one can see a dark contrast "mountain-like" marking indicated by blue arrows. The right edge of the mountain-like markings corresponds to the striation location indicated by the red arrows. Similar markings have been reported by Nishikawa et al.[57] They performed TEM and electron backscattered diffraction (EBSD) analyses beneath the fracture surface of a low carbon steel fatigued under gaseous hydrogen and found a similar type of mountain-like marking corresponding to striation. The difference in TEM image contrast is due to lattice distortion caused by local plastic strain shown by EBSD analysis. Thus, the mountain-like markings may be a region with higher plastic strain compared to
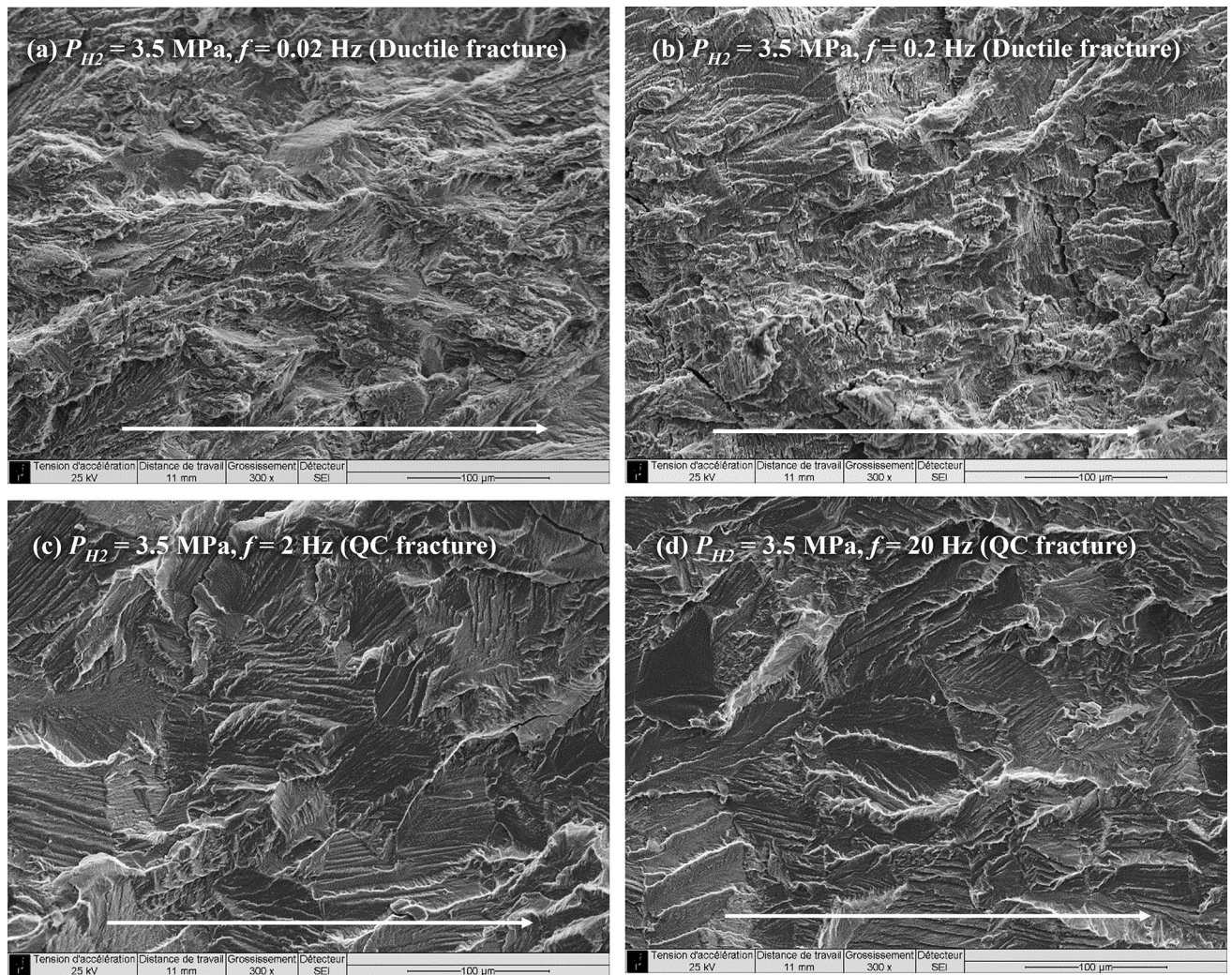
Fig. 4—Fracture surfaces of the ΔK-constant tests (at $\Delta K = 20$ MPa $\times m^{1/2}$) in hydrogen at $P_{H_2} = 3.5$ MPa and $f = 0.02$ (*a*), 0.2 (*b*), 2 (*c*), and 20 Hz (*d*). The crack propagation direction is from left to right.

the other part. As with the present observation (Figure 7(b)), they also observed slip bands (linear markings leading to striation). In contrast, at $f = 0.02$ Hz, foil was extracted (Figure 8(c)) from the ductile transgranular fracture area. A clear dislocation cell structure is observed throughout the foil, as shown in Figure 8(d). While not shown here, the dislocation structures in nitrogen at 20 and 0.02 Hz were confirmed as a cell structure similar to that presented in Figure 8(d).

TEM observations make it possible to correlate the dislocation structure with the FCGR as presented in Figure 2 at both hydrogen gas pressures: a brittle QC fracture is associated with randomly distributed dislocation tangles (DT) and ductile fracture with a dislocation cell (DC) structure, respectively. Furthermore, a low level of microscopic crack tip plasticity is related to the FCG enhancement, which is consistent with the macroscopic cyclic crack tip plasticity observed in the surface topography measurement.

IV. DISCUSSION

A. *Mechanism of FCG Enhancement by Hydrogen*

This study clearly demonstrated that hydrogen-induced FCGR acceleration is strongly associated with a reduction of cyclic crack tip plasticity. A crack tip plasticity reduction has also been confirmed at the microscopic scale immediately beneath the fracture surface evidenced by the TEM observations as well as at the mesoscopic scale analyzed by the interferometric microscopy. A research group at Kyushu University [2,29,44,45,52,60–62] has actively investigated cyclic plastic deformation near the crack path in HAFCG using an optical microscopy. They revealed that FCG enhancement by a hydrogen environment or a hydrogen-charged state is accompanied by the localization of plastic deformation near the crack path in austenitic stainless steel,[29,60,61] Cr-Mo steel,[62] and low carbon steel.[28,44,45] They also characterized the localization of crack tip plasticity by fracture surface morphology.[29,60] Specifically, they measured the fracture surface
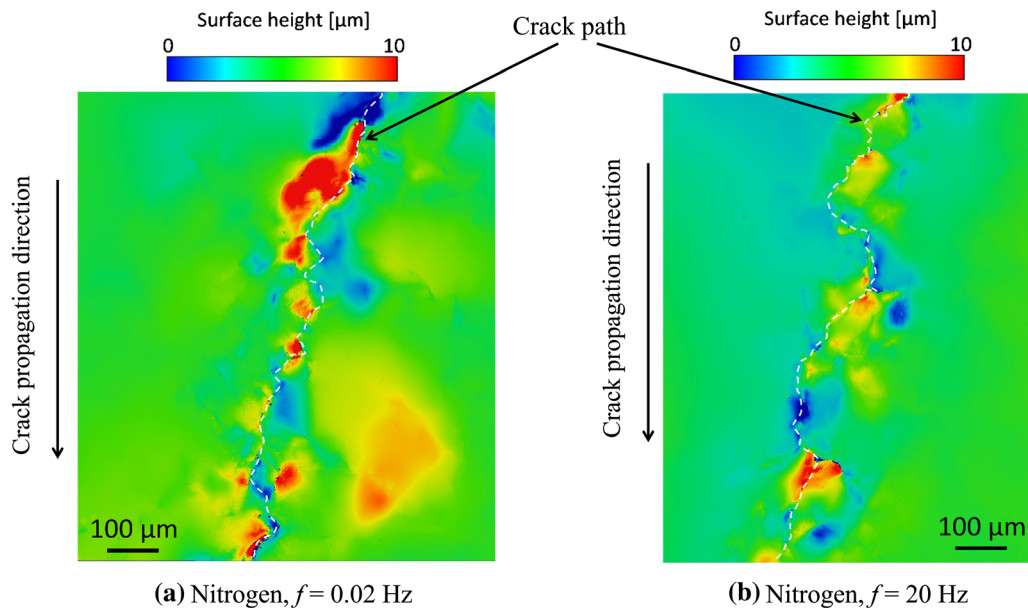
Fig. 5—Surface topography (height variation) of the side-surface near the crack path of the ΔK-constant test (at $\Delta K = 20$ MPa $\times$ $m^{1/2}$) in nitrogen ($P_{N_2} = 35$ MPa) at $f = 0.02$ (*a*) and 20 (*b*) Hz. Crack propagation direction is from top to bottom. The crack path is indicated by the white dashed line.

morphology with striations using stereographic SEM analysis. They concluded that the presence of hydrogen reduces crack tip blunting and surface undulation of striations. Besides, Birenis *et al.*[31,32] performed TEM observations of the dislocation structure formed under HAFCG in a pure iron and observed dislocation tangles without a clear cell structure. This is consistent with the present observations. They also confirmed the crack tip plasticity reduction by grain reference orientation deviation (GROD) mapping, which visualizes the plastic strain distribution near the crack path.

The mechanism of the HAFCG enhancement associated with a crack tip plasticity reduction may be explained referring to a hydrogen-induced cyclic cleavage model [27,31,32] as follows. The highly accumulated solute hydrogen atoms in front of the crack tip limit the plasticity development and blunting of the crack tip due to the hydrogen effect suppressing dislocation mobility.[37–42] Consequently, when both the stress intensity and hydrogen concentration ahead of the crack tip reach critical levels, cleavage fracture occurs because of a bonding energy reduction of matrix atoms by hydrogen (*i.e.*, the HEDE mechanism). The critical condition in terms of hydrogen concentration and stress state is also recognized by Djukic *et al.*[4,16,17] They determined the critical hydrogen concentration as a function of applied stress level triggering ductile to brittle fracture transition accompanied by a drop of the material strength. It has to be noted that, even if the final fracture process is decohesion (namely HEDE), a different interpretation is still possible for the process to achieve the critical hydrogen concentration and the crack tip plasticity reduction (or maybe plasticity localization). Djukic *et al.*[4,16] and Martin *et al.*[33] advocate that locally enhanced plasticity (dislocation nucleation and/or mobility) due to the HELP mechanism mediates the reaching of the critical level of hydrogen concentration ahead of the crack tip, resulting in the activation of the HEDE mechanism (*i.e.*, the HELP-mediated HEDE model).

B. *Interpretation of the Peculiar Dependency of HAFCG on Low f*

The observed HAFCG behavior clearly depends on hydrogen gas pressure P_{H_2} and loading frequency f. A mechanism accounting for such a dependency is discussed here. In the previous study,[27] the HAFCG behavior within the relatively high f range was well interpreted based on the hydrogen distribution ahead of the crack tip, as briefly described below.

From the viewpoint of P_{H_2} dependence, ΔK triggering the FCGR enhancement (*i.e.*, ΔK_{tr}) decreases by increasing the hydrogen gas pressure. Here, the hydrogen concentration at the crack tip C_s is theoretically proportional to P_{H_2} according to Sievert's law.[63] Also, ΔK_{tr} depends on the hydrogen gas pressure (Figure 1). By considering these facts, it can be assumed that C_s is a controlling factor of the shift of ΔK_{tr}. This relationship may explain the dependence of ΔK_{tr} on P_{H_2} in the framework of the hydrogen-induced cyclic cleavage model. Since the model assumes that the cleavage fracture requires critical levels of hydrogen gas pressure and stress intensity at the crack tip, if hydrogen gas pressure is high (*i.e.*, C_s is high), the critical condition is easily accomplished with a low level of stress intensity at the crack tip. On the contrary, if the hydrogen gas pressure is low (*i.e.*, C_s becomes low), a high level of stress intensity at the crack tip is required to activate the cleavage fracture.[24,27] The synergistic condition of the
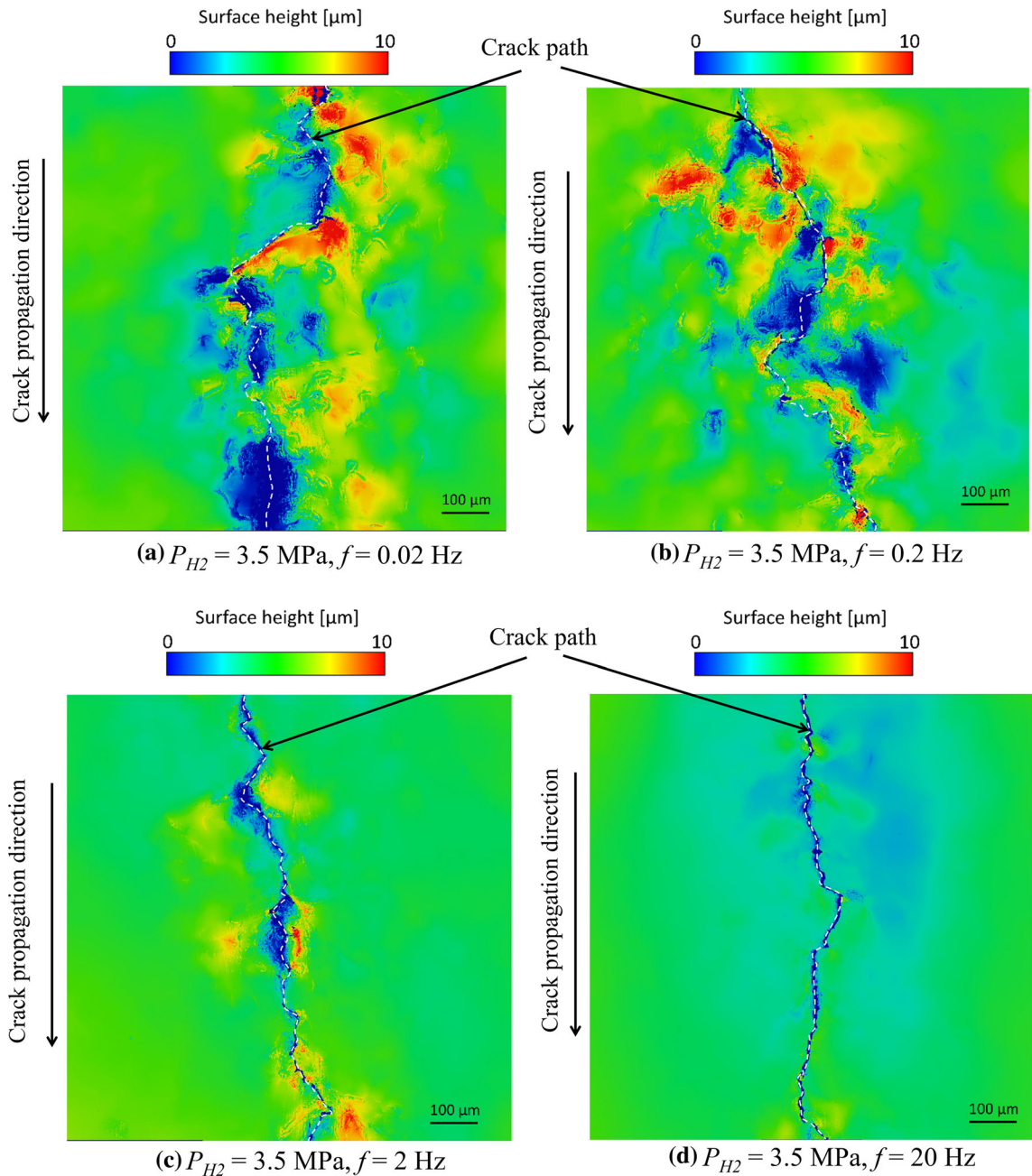
Fig. 6—Surface topography (height variation) of the side surface near the crack path of the ΔK-constant test (at $\Delta K = 20$ MPa $\times$ $m^{1/2}$) in hydrogen at $P_{H_2} = 3.5$ MPa and $f = 0.02$ (*a*), 0.2 (*b*), 2 (*c*), and 20 (*d*) Hz. Crack propagation direction is from top to bottom. The crack path is indicated by the white dashed line.

critical hydrogen concentration and the stress intensity level should be further investigated and quantitatively identified in the future.

In terms of f dependency, the magnitude of FCGR enhancement with fixed ΔK in the accelerated regime increases by decreasing f until reaching saturation. If the loading frequency decreases, the penetration depth $(D/f)^{1/2}$ (a distance from the crack tip to a location at which $C_H/C_s = 0.5$, where D the diffusivity coefficient and C_s the saturated hydrogen concentration on the surface) is theoretically expected to increase without considering trapping. According to the hydrogen-induced cyclic

cleavage model, a deeper hydrogen penetration ahead of the crack tip allows a longer cleavage crack advancement resulting in higher FCGR.

In addition to this f dependency, this study has revealed a peculiar HAFCG behavior at low f. Typically, the magnitude of FCGR enhancement reaches an upper limit by decreasing f down to a specific value, but further decreasing f causes the rapid decrease in FCGR. At the same time, the hydrogen effect reducing crack tip plasticity disappears. The fracture mode becomes ductile as same as in inert environment, and dislocation cells are formed in the bulk, indicating highly cumulated plastic strain.
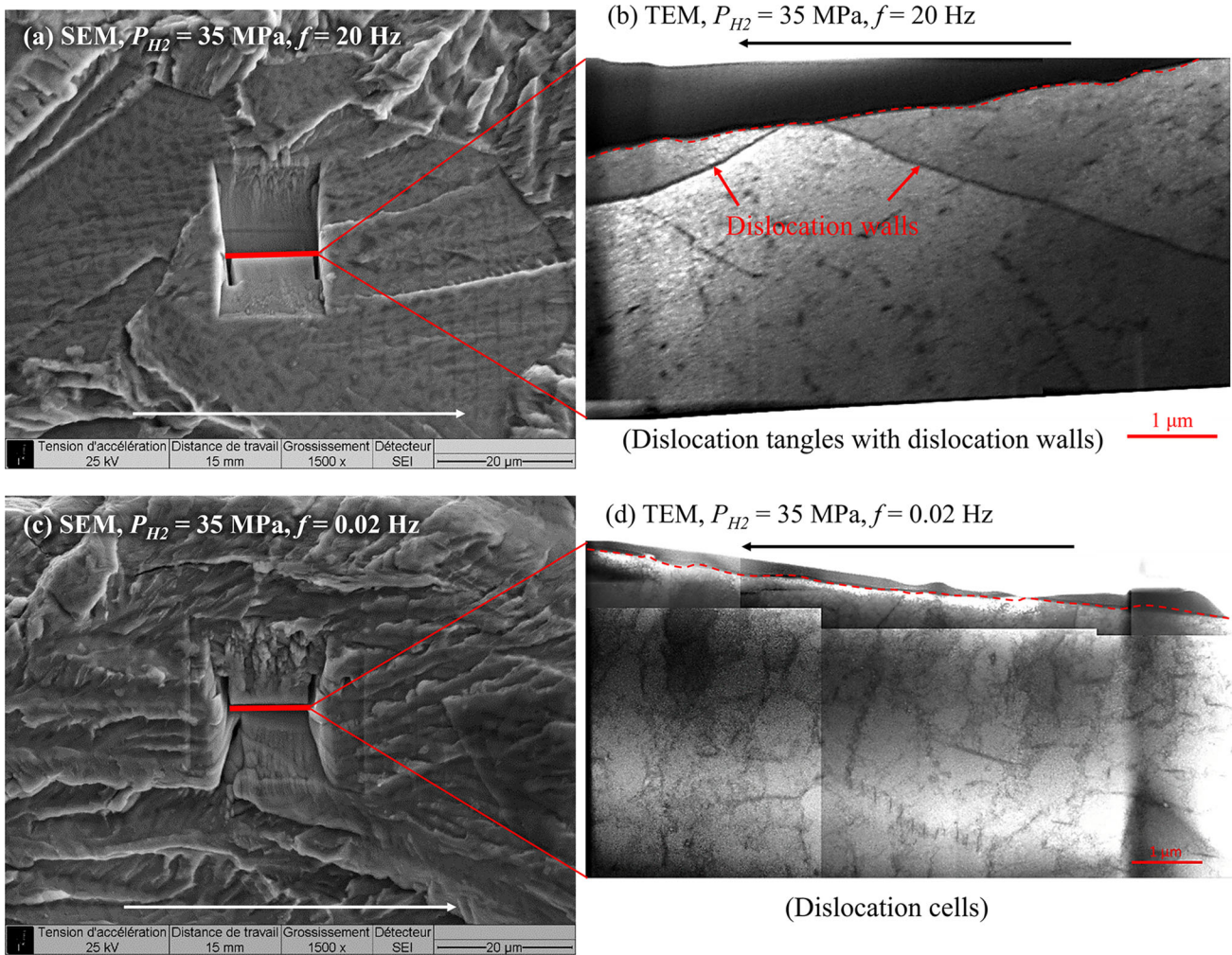
Fig. 7—ΔK-constant tests (at $\Delta K = 20$ MPa $\times m^{1/2}$) in hydrogen at $P_{H_2} = 35$ Mpa, $f = 20$ Hz (*a*) and (*b*), and 0.02 Hz (*c*) and (*d*). Images (a) and (c) are SEM images of the fracture surface around the location of the sample extraction indicated by the red line. Images (b) and (d) are TEM images of the lamella. Red dashed line indicates the location of the fracture surface. Black arrow indicates the crack propagation direction (Color figure online).

A similar finding has been made by Yoshikawa *et al.*[44,45] regarding this attenuation of the hydrogen effects at low *f* based on their series of FCG tests on a low carbon steel with a wide range of hydrogen gas pressure and loading frequency. Their results of FCGRs at relatively low hydrogen gas pressures exhibit a reversal effect of loading frequency similar to the one observed in this study (Figure 2). Yoshikawa *et al.*[44,45] theoretically estimated the gradient of hydrogen concentration in the vicinity of the crack tip expressed by:

$$\left(\frac{P_{H_2} \times f}{2D}\right)^{1/2} \propto (P_{H_2} \times f)^{1/2} \qquad [1]$$

The definition of this term is the average gradient of hydrogen concentration within a penetration depth $(D/f)^{1/2}$. By rearranging the FCGR data as a function of $(P_{H_2} \times f)^{1/2}$, Yoshikawa *et al.* have found that the attenuation of FCGR enhancement at $\Delta K = 30$ MPa $\times m^{1/2}$ occurs if $(P_{H_2} \times f)^{1/2}$ is < 0.2 (MPa/s)$^{1/2}$, regardless of the hydrogen gas pressure.[44,45]

To examine the relevance of this relationship to the present result, FCGRs in hydrogen are plotted as a function of the $(P_{H_2} \times f)^{1/2}$ in Figure 9. This figure clearly demonstrates that the FCGR enhancement at both hydrogen gas pressures occurs at approximately the same value of $(P_{H_2} \times f)^{1/2} \sim 2$ (MPa/s)$^{1/2}$. This indicates that the hydrogen gradient $(P_{H_2} \times f)^{1/2}$ is an effective criterion for the HAFCGR enhancement onset of Armco iron. The reason for the discrepancy of $(P_{H_2} \times f)^{1/2}$ between the present study and the one of Yoshikawa *et al.* may be related to the difference in yield strength of the materials. It is known that the higher the yield strength is, the lower the hydrogen-induced crack growth threshold K_{th}.[64] Since Armco iron and the low carbon steel used by Yoshikawa *et al.* have different yield strength of 170 and 360 MPa, respectively, this difference causes the difference in hydrogen gradient required for the onset of hydrogen-enhanced FCG.

Yoshikawa *et al.*[44,45] also observed a clear reduction in plastic deformation near the crack tip that occurs in the presence of a high hydrogen gradient. On the other
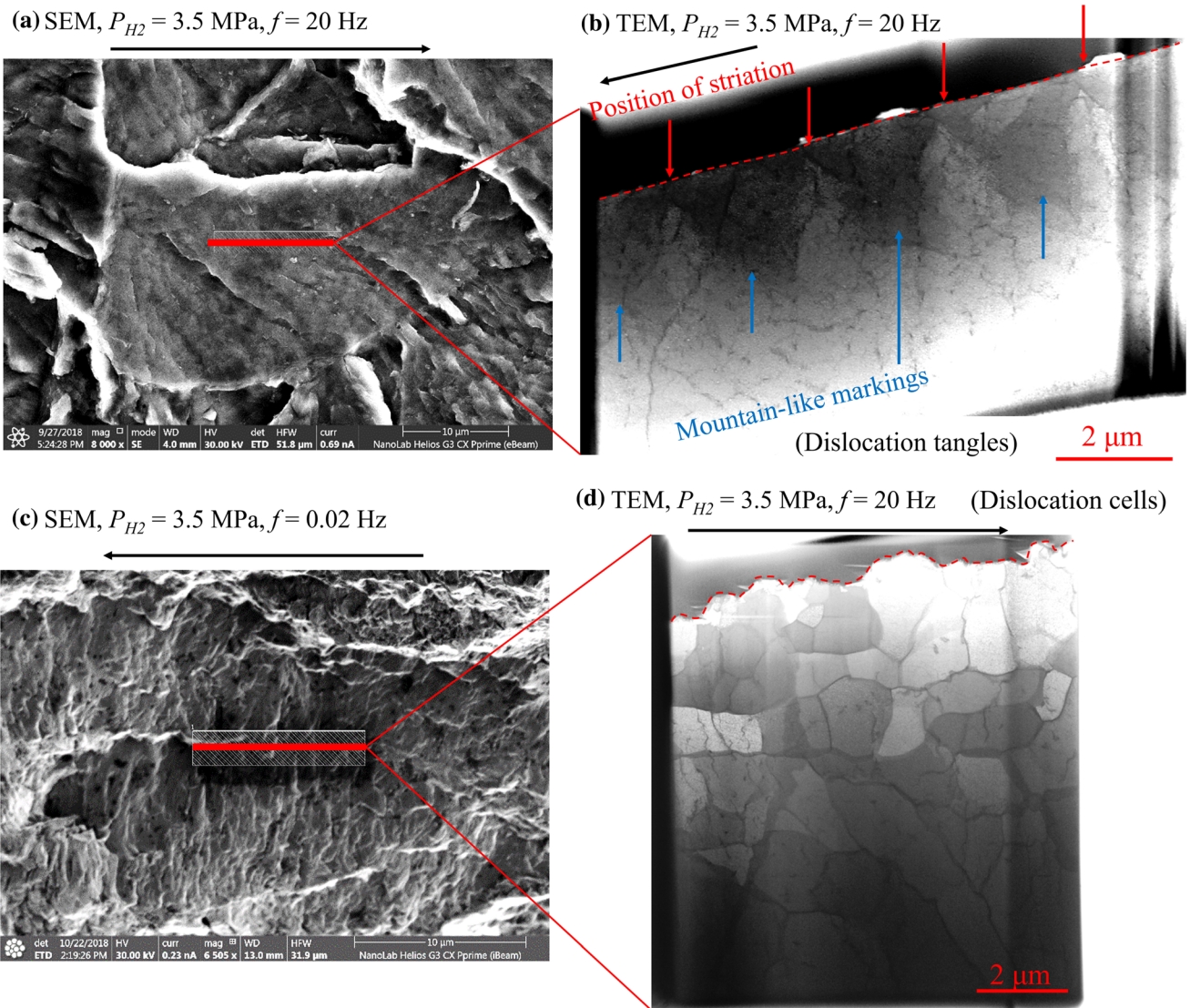
(a) SEM, P_{H2} = 3.5 MPa, f = 20 Hz

(b) TEM, P_{H2} = 3.5 MPa, f = 20 Hz

Position of striation

Mountain-like markings

(Dislocation tangles)

2 μm

(c) SEM, P_{H2} = 3.5 MPa, f = 0.02 Hz

(d) TEM, P_{H2} = 3.5 MPa, f = 20 Hz   (Dislocation cells)

2 μm

Fig. 8—ΔK-constant tests (at $\Delta K = 20$ MPa $\times m^{1/2}$) in hydrogen at $P_{H_2} = 3.5$ MPa, $f = 20$ Hz (*a*) and (*b*), and 0.02 Hz (*c*) and (*d*). Images (a) and (c) are SEM images of the fracture surface around the location of the sample extraction indicated by the red line. Images (b) and (d) are TEM images of the lamella. Red dashed line indicates the location of the fracture surface. Black arrow indicates the crack propagation direction (Color figure online).

hand, with a low level of hydrogen gradient without FCG enhancement, the extent of crack tip plasticity is the same level as in air, consistent with the present result. However, they did not provide a clear explanation why the hydrogen gradient is so important for the activation of the hydrogen effect in their literature.

The hydrogen effect attenuation at low f may be understood considering a velocity balance between hydrogen atoms and mobile dislocations, which was highlighted by Takai *et al*.[65,66] They measured a hydrogen desorption rate of pure iron and Inconel 625 during tensile deformation at various strain rates. As a result, the amount of desorbed hydrogen in pure iron increased by increasing the strain rate from 4.2×10^{-5} to 4.2×10^{-4} s^{-1} and reached the maximum amount (16 pct of the initial hydrogen content) at the strain rate of 4.2×10^{-4} s^{-1}. The amount of desorbed hydrogen inversely decreased by increasing the strain rate from 4.2

$\times 10^{-4}$ to 4.2×10^{-3} s^{-1}. Takai *et al*. concluded that if a velocity is balanced between hydrogen atoms and dislocations, their interaction is maximized, and the dislocations deliver the maximum amount of hydrogen.

The reason why the hydrogen gradient controls the HAFCG enhancement may be interpreted by the above-mentioned framework. As a hydrogen flux J is a function of the hydrogen concentration gradient,[67] a higher hydrogen gradient leads to higher hydrogen flux ahead of the crack tip. According to the theory of Takai *et al*., it is considered that a large number of diffusing hydrogen atoms driven by a high hydrogen concentration gradient is a necessary condition for the interaction between hydrogen atoms and mobile dislocations because the mobile dislocations and the diffusing hydrogen atoms may interact when their velocities are close. If the hydrogen concentration gradient is very small (*i.e.*, a hydrogen saturation), the diffusion of hydrogen atoms is
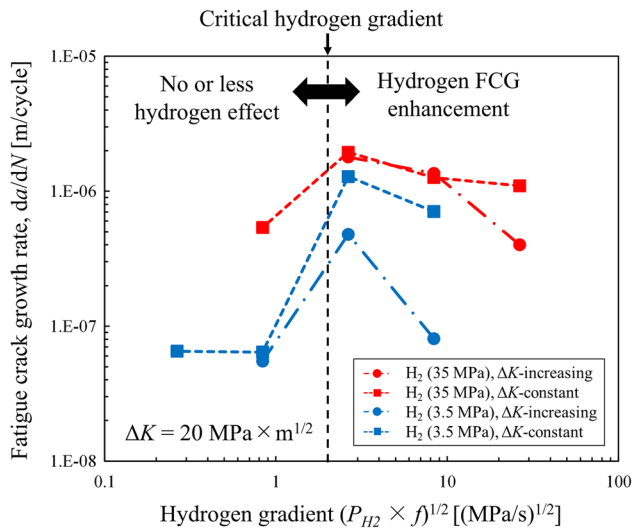
Fig. 9—Relationship between HAFCGR and the hydrogen gradient $(P_{H_2} \times f)^{1/2}$ at $\Delta K = 20$ MPa $\times$ m$^{1/2}$.

marginal; consequently, there is no interaction between hydrogen and dislocation. This assumption may explain the importance of the hydrogen gradient that controls HAFCG enhancement. A similar interpretation was recently proposed by Wan et al.[68] considering the thermal activation energy associated with the dislocation motion that depends on the strain rate. However, it is still unclear at this stage how the gradient parameter can account for the interaction between dislocations and hydrogen atoms because the dislocation and hydrogen velocities in the vicinity of fatigue crack tip have not yet been quantitatively investigated. Quantitative investigation of this issue is desirable in future work to verify the above assumptions and to clarify the interaction mechanism between hydrogen and dislocations.

On the other hand, Somerday et al.[51] suggested that the attenuation of the hydrogen effect at low f is caused by an oxidation of the crack surface that prevents an absorption of hydrogen from the crack tip. They argued that a certain amount of oxygen contained in a hydrogen gas may induce f dependency. Their FCG tests in X52 line pipe steel showed that with even a very small amount of oxygen of 10 ppm, hydrogen effect attenuation occurred. Thus, it is also possible that oxygen affects the present case. In contrast, Matsunaga et al.[54] have denied this explanation by referring to their experimental study of the FCG tests in hydrogen-charged 304 stainless steel. In their tests, the attenuation of the hydrogen effect at very low loading frequency was demonstrated without an influence of oxygen. Since the microstructure of material and the hydrogen charging method are different between those two studies, neither can be concluded at this stage. This point needs further investigation in a prospective study. The transition of fracture mode between ductile and brittle under specific conditions is also considered by the HELP + HEDE model proposed by Djukic et al.,[4,16] describing the HE mechanism as a coexistence of HELP and HEDE mechanisms as synergistic or independent action. This model interprets the transition of the dominant HE mechanism from the plasticity-mediated hydrogen effect to the decohesion-controlled mechanism as a function of the hydrogen concentration and applied stress levels, and the transition is triggered by reaching a critical hydrogen concentration.

It has to be noted that another interesting feature found in the present fracture surface observation at P_{H_2} = 35 MPa and f = 0.02 Hz (Figure 3(a)) is the larger size of cleavage-like facets compared to higher f. Since the hydrogen flux at the crack tip is large if the loading frequency is 0.2 Hz or more, the effect of hydrogen causing cleavage in the grain is strong. Then, the cleavage fracture may occur simultaneously in several planes with a specific orientation with weak atomic bonds in a grain (e.g., {100} plane for bcc material). This is evidenced by the investigation of the relevance between the cleavage crack path and adjacent grain orientation by Birenis et al.[31,36] In this case, the adjacent cleavage surfaces are possibly connected to each other, resulting in a step-like fracture surface as seen in Figures 3(b) through (d). On the other hand, when the frequency is lowered to 0.02 Hz, the hydrogen effect causing cleavage is relatively weak as the hydrogen flux decreases. Thus, among the several potential cleavage planes in a grain, the cleavage fracture occurs along the weakest single plane. Therefore, large cleavage facets are formed on a fracture surface as shown in Figure 3(a). Though it is still speculation, the effect of hydrogen might disappear if the frequency is lowered below 0.02 Hz at P_{H_2} = 35 MPa, and the fracture mode might change to brittle like in the cases of P_{H_2} = 3.5 MPa, f = 0.2, and 0.02 Hz. This hypothesis needs to be examined in future research.

C. Criteria for HAFCG Enhancement

One of the beneficial outcomes from this study is the identification of three criteria of the HAFCG enhancement: an upper limit of HAFCGR, ΔK_{tr}, and $(P_{H_2} \times f)^{1/2}$. The three criteria are expected to help in the fatigue design and fatigue life predictions of hydrogen-related equipment. The upper limit of the HAFCG rate can be considered a maximum possible FCGR at any loading frequency under a hydrogen environment. This value allows us to estimate a minimum fatigue life of products and to determine the periods of product use and replacement. Besides, ΔK_{tr} (as a function of P_{H_2}) and $(P_{H_2} \times f)^{1/2}$ could be considered as criteria for fatigue life reduction. These criteria are useful to determine the specific usage condition of materials under a hydrogen environment without critical degradation of the fatigue life.

The phenomena represented by ΔK_{tr} and $(P_{H_2} \times f)^{1/2}$ as the criteria of the HAFCG enhancement onset are considered different because of the following two findings. The first evidence is that the fracture mode is different: the fracture mode in the low ΔK range ($\Delta K < \Delta K_{tr}$) is intergranular [27]; meanwhile, the one in the low hydrogen gradient $\left((P_{H_2} \times f)^{1/2} < 2\right)$ is ductile transgranular (and QC). The second evidence is that the shift

of ΔK_{tr} cannot be explained by $(P_{H_2} \times f)^{1/2}$. For example, the two testing conditions, P_{H_2} = 35 MPa, f = 0.2 Hz and P_{H_2} = 3.5 MPa, f = 2 Hz, are characterized by the same value of $(P_{H_2} \times f)^{1/2}$ = 2 $(\text{MPa/s})^{1/2}$. However, the values of ΔK_{tr} are different as shown in Figure 1. These values of ΔK_{tr} should be consistent if ΔK_{tr} was also controlled by $(P_{H_2} \times f)^{1/2}$. Therefore, the physical phenomena triggering the FCG enhancement by satisfying ΔK_{tr} or $(P_{H_2} \times f)^{1/2}$ are probably different. The physical meanings of these parameters need to be further investigated in the future.

V. CONCLUSIONS

To characterize the f dependency of HAFCG and to understand its mechanism, the FCG tests in Armco iron under a gaseous hydrogen environment were conducted at various f and P_{H_2}. The influence of hydrogen on crack tip plasticity was identified by means of interferometric microscopy and TEM. The main conclusions are summarized below.

1. The HAFCGR increases by decreasing f down to the critical values, which are f = 2 Hz in case of P_{H_2} = 3.5 MPa and f = 0.2 Hz in case of P_{H_2} = 35 MPa. The fracture mode is brittle quasi-cleavage fracture if f is above the critical value. On the other hand, if f is below the critical values, the fracture mode becomes more a ductile fracture or QC fracture with larger size of cleavage-like facets, which might be related to a less intense hydrogen effect.
2. The crack tip plasticity is limited because of the presence of hydrogen if f is higher than the critical value; meanwhile, the crack tip plasticity becomes prominent at the same level as in an inert environment if f is lower than the certain value. These results show that the influence of hydrogen on both FCGR and crack tip plasticity is limited at very low f.
3. The reversal f dependency of HAFCG seems to be governed by a gradient of hydrogen concentration ahead of the crack tip simply represented by $(P_{H_2} \times f)^{1/2}$.
4. The mechanism of f dependency of HAFCG may be understood by considering the balance of velocities between hydrogen atoms and mobile dislocations. However, since many unclear parts remain in this hypothesis, further investigation is necessary on a dynamic interaction between hydrogen and crack tip plasticity as a function of f and hydrogen concentration. At the same time, it is necessary to keep considering other possible interpretations such as the synergetic effects of HELP and HEDE mechanisms explaining a ductile to brittle transition.
5. Three criteria characterizing HAFCG enhancement have been identified: an upper limit of HAFCGR, ΔK_{tr} (as a function of P_{H_2}), and $(P_{H_2} \times f)^{1/2}$. These criteria are expected to be useful for a safety fatigue design for hydrogen-related equipment.

REFERENCES:

1. G. Hénaff, G. Odemer, and A. Tonneau-Morel: *Int. J. Fatigue*, 2007, vol. 29, pp. 1927–40.
2. Y. Murakami and S. Matsuoka: *Eng. Fract. Mech.*, 2010, vol. 77, pp. 1926–40.
3. S.P. Lynch: *Metall. Mater. Trans. A*, 2012, vol. 44A, pp. 1209–29.
4. M.B. Djukic, G.M. Bakic, V. Sijacki Zeravcic, A. Sedmak, and B. Rajicic: *Eng. Fract. Mech.*, 2019, vol. 216, p. 106528.
5. N. Nanninga, A. Slifka, Y. Levy, and C. White: *J. Res. Natl. Inst. Stand. Technol.*, 2010, vol. 115, p. 437.
6. W.H. Johnson: *Proc. R. Soc. Lond.*, 1874, vol. 23, pp. 168–79.
7. R.A. Oriani and P.H. Josephic: *Scr. Metall.*, 1972, vol. 6, pp. 681–88.
8. R.A. Oriani: *Berichte der Bunsengesellschaft Technol. Asp.*, 1972, vol. 76, pp. 848–57.
9. H.K. Birnbaum and P. Sofronis: *Mater. Sci. Eng. A*, 1994, vol. 176, pp. 191–202.
10. S.P. Lynch and N.E. Ryan: in *Proc. Second Int. Congr. Hydrog. Met.*, 1977, pp. 369–76.
11. M. Nagumo: *ISIJ Int.*, 2001, vol. 41, pp. 590–98.
12. L. Jemblie, V. Olden, and O.M. Akselsen: *Int. J. Hydrogen Energy*, 2017, https://doi.org/10.1016/j.ijhydene.2017.02.211.
13. L. Jemblie, O.M. Akselsen, and V. Olden: *Philos. Trans. R. Soc. A Math. Phys. Eng. Sci.*, 2017, vol. (in press), pp. 1–16.
14. A. Tehranchi and W.A. Curtin: *Eng. Fract. Mech.*, 2019, vol. 216, p. 106502.
15. S. Taketomi, R. Matsumoto, and S. Hagihara: *ISIJ Int.*, 2017, vol. 57, pp. 2058–64.
16. M.B. Djukic, V. Sijacki-Zeravcic, G.M. Bakic, A. Sedmak, and B. Rajicic: *Eng. Fail. Anal.*, 2015, vol. 58, pp. 485–98.
17. M.B. Djukic, G.M. Bakic, V.S. Zeravcic, A. Sedmak, and B. Rajicic: *Corrosion*, 2016, vol. 72, pp. 943–61.
18. M. Koyama, C.C. Tasan, E. Akiyama, K. Tsuzaki, and D. Raabe: *Acta Mater.*, 2014, vol. 70, pp. 174–87.
19. Y. Hu, C. Dong, H. Luo, K. Xiao, P. Zhong, and X. Li: *Metall. Mater. Trans. A Phys. Metall. Mater. Sci.*, 2017, vol. 48, pp. 4046–57.
20. J. Rehrl, K. Mraczek, A. Pichler, and E. Werner: *Mater. Sci. Eng. A*, 2014, vol. 590, pp. 360–67.
21. D. Sasaki, M. Koyama, and H. Noguchi: *Mater. Sci. Eng. A*, 2015, vol. 640, pp. 72–81.
22. A. Nagao, M. Dadfarnia, B.P. Somerday, P. Sofronis, and R.O. Ritchie: *J. Mech. Phys. Solids*, 2018, vol. 112, pp. 403–30.
23. B.S. Kumar, V. Kain, M. Singh, and B. Vishwanadh: *Mater. Sci. Eng. A*, 2017, vol. 700, pp. 140–51.
24. Y. Ogawa, D. Birenis, H. Matsunaga, O. Takakuwa, J. Yamabe, Ø. Prytz, and A. Thøgersen: *Mater. Sci. Eng. A*, 2018, vol. 733, pp. 316–28.
25. L. Wan, W. Tong, A. Ishii, J. Du, and N. Ishikawa: *Int. J. Plast.*, 2018, pp. 1–26.
26. S. Wang, M.L. Martin, I.M. Robertson, and P. Sofronis: *Acta Mater.*, 2016, vol. 107, pp. 279–88.
27. T. Shinko, G. Henaff, D. Halm, G. Benoit, G. Bilotta, and M. Arzaghi: *Int. J. Fatigue*, 2018, https://doi.org/10.1016/j.ijfatigue.2018.12.009.

28. S. Matsuoka, N. Tsutsumi, and Y. Murakami: *Trans Japan Soc. Mech. Eng. Ser. A (in Japanese)*, 2008, vol. 74, pp. 1528–37.
29. Y. Murakami, T. Kanezaki, Y. Mine, and S. Matsuoka: *Metall. Mater. Trans. A*, 2008, vol. 39A, pp. 1327–39.
30. H. Nishikawa, Y. Oda, and H. Noguchi: *J. Solid Mech. Mater. Eng.*, 2011, vol. 5, pp. 370–85.
31. D. Birenis, Y. Ogawa, H. Matsunaga, O. Takakuwa, J. Yamabe, Ø. Prytz, and A. Thøgersen: *Acta Mater.*, 2018, vol. 156, pp. 245–53.
32. D. Birenis, Y. Ogawa, H. Matsunaga, O. Takakuwa, J. Yamabe, Ø. Prytz, and A. Thøgersen: *MATEC Web Conf.*, 2018, vol. 165, p. 03010.
33. M.L. Martin, M. Dadfarnia, A. Nagao, S. Wang, and P. Sofronis: *Acta Mater.*, 2019, vol. 165, pp. 734–50.
34. T.J. Marrow, P.J. Cotterill, and J.E. King: *Acta Metall. Mater.*, 1992, vol. 40, pp. 2059–68.
35. T. Shinko, G. Hénaff, D. Halm, and G. Benoit: *MATEC Web Conf.*, 2018, vol. 165, p. 03006.
36. D. Birenis, Y. Ogawa, H. Matsunaga, O. Takakuwa, J. Yamabe, Ø. Prytz, and A. Thøgersen: *Mater. Sci. Eng. A*, 2019, vol. 756, pp. 396–404.
37. S. Taketomi, R. Matsumoto, and N. Miyazaki: *J. Mater. Res.*, 2011, vol. 26, pp. 1269–78.
38. N. Taketomi, S., Imanishi, S., Matsumoto, R., Miyazaki: in *13th Int. Conf. Fract.*, 2013, pp. 16–21.
39. T. Hajilou, Y. Deng, B.R. Rogne, N. Kheradmand, and A. Barnoush: *Scr. Mater.*, 2017, vol. 132, pp. 17–21.
40. H. Matsui, H. Kimura, and S. Moriya: *Mater. Sci. Eng.*, 1979, vol. 40, pp. 207–16.
41. S. Moriya, H. Matsui, and H. Kimura: *Mater. Sci. Eng.*, 1979, vol. 40, pp. 217–25.
42. H. Matsui, H. Kimura, and A. Kimura: *Mater. Sci. Eng.*, 1979, vol. 40, pp. 227–34.
43. Y. Ogawa, D. Birenis, H. Matsunaga, O. Takakuwa, J. Yamabe, Ø. Prytz, and A. Thøgersen: *MATEC Web Conf.*, 2018, vol. 165, p. 03011.
44. M. Yoshikawa, T. Matsuo, N. Tsutsumi, H. Matsunaga, and S. Matsuoka: *Trans. JSME (in Japanese)*, 2014, vol. 80, p. SMM0254.
45. J. Yamabe, M. Yoshikawa, H. Matsunaga, and S. Matsuoka: *Procedia Struct. Integr.*, 2016, vol. 2, pp. 525–32.
46. Z. Sun, C. Moriconi, G. Benoit, D. Halm, and G. Henaff: *Metall. Mater. Trans. A*, 2012, vol. 44A, pp. 1320–30.
47. G. Bilotta, M. Arzaghi, G. Hénaff, G. Benoit, and D. Halm: *Vol. 6B Mater. Fabr.*, 2016, p. V06BT06A026.
48. G. Bilotta, M. Arzaghi, G. Benoit, D. Halm, G. Henaff, and T. Shinko: in *Proc. Int. Hydrog. Conf. (IHC 2016) Mater. Perform. Hydrog. Environ.*, 2016, pp. 1–10.
49. Y. Takeo and S. Kiyoshi: *Eng. Fract. Mech.*, 1976, https://doi.org/10.1016/0013-7944(76)90078-3.
50. G. Bilotta, M. Arzaghi, G. Hénaff, G. Benoit, C. Moriconi, and D. Halm: in *Volume 6B: Materials and Fabrication*, ASME, 2014, p. V06BT06A014.
51. B.P. Somerday, P. Sofronis, K.A. Nibur, C.S. Marchi, and R. Kirchheim: *Acta Mater.*, 2013, vol. 61, pp. 6153–70.
52. S. Matsuoka, H. Tanaka, N. Homma, and Y. Murakami: *Int. J. Fract.*, 2011, vol. 168, pp. 101–12.
53. A. Macadre, M. Artamonov, S. Matsuoka, and J. Furtado: *Eng. Fract. Mech.*, 2011, vol. 78, pp. 3196–3211.
54. H. Matsunaga, T. Nakashima, K. Yamada, T. Matsuo, J. Yamabe, and S. Matsuoka: in *Vol. 6B Mater. Fabr.*, 2016, p. V06BT06A031.
55. H. Matsunaga, O. Takakuwa, J. Yamabe, and S. Matsuoka: *Philos. Trans. R. Soc. A Math. Phys. Eng. Sci.*, 2017, vol. 375, p. 20160412.
56. Y. Ogawa, D. Birenis, H. Matsunaga, A. Thøgersen, Ø. Prytz, O. Takakuwa, and J. Yamabe: *Scr. Mater.*, 2017, vol. 140, pp. 13–17.
57. H. Nishikawa, Y. Oda, Y. Takahashi, and H. Noguchi: *J. Solid Mech. Mater. Eng.*, 2011, vol. 5, pp. 179–90.
58. O. Takakuwa, Y. Ogawa, S. Okazaki, M. Nakamura, and H. Matsunaga: *Corros. Sci.*, 2020, p. 108558.
59. Y. Deng, T. Hajilou, D. Wan, N. Kheradmand, and A. Barnoush: *Scr. Mater.*, 2017, vol. 127, pp. 19–23.
60. T. Kanezaki, C. Narazaki, Y. Mine, S. Matsuoka, and Y. Murakami: *Int. J. Hydrogen Energy*, 2008, vol. 33, pp. 2604–19.
61. Y. Murakami, T. Kanezaki, and Y. Mine: *Metall. Mater. Trans. A Phys. Metall. Mater. Sci.*, 2010, vol. 41A, pp. 2548–62.
62. T. Matsuo, S. Matsuoka, and Y. Murakami: in *18th European Conference on Fracture*, Dresden, Germany, 2010, pp. 1–8.
63. Y. Fukai: *The Metal-Hydrogen System*, vol. 21, 2nd edn., Springer, New York, 2005.
64. K.A. Nibur, B.P. Somerday, C.S. Marchi, J.W. Foulk, III, M. Dadfarnia, and P. Sofronis: *Metall. Mater. Trans. A-Phys. Metall. Mater. Sci.*, 2013, vol. 44A, pp. 248–69.
65. H. Shoda, H. Suzuki, K. Takai, and Y. Hagihara: *Tetsu-to-Hagane*, 2009, vol. 95, pp. 573–81.
66. K. Takai, H. Shoda, H. Suzuki, and M. Nagumo: *Acta Mater.*, 2008, vol. 56, pp. 5158–67.
67. P. Sofronis and R.M. McMeeking: *J. Mech. Phys. Solids*, 1989, vol. 37, pp. 317–50.
68. D. Wan, Y. Deng, J.I.H. Meling, A. Alvaro, and A. Barnoush: *Acta Mater.*, 2019, vol. 170, pp. 87–99.